Self-Assembly in Complex Mixed Surfactant Solutions: The Impact of Dodecyl Triethylene Glycol on Dihexadecyl Dimethyl Ammonium Bromide

I. Tucker,*,† J. Penfold,‡,§ R. K. Thomas,§ I. Grillo,|| D. F. R. Mildner,⊥ and J. G. Barker⊥

Unilever Research and Development Port Sunlight, Quarry Road East, Bebington Wirral CH63 3JW, U.K., STFC Rutherford Appleton Laboratory, Chilton, Didcot, Oxon OX11 0QX, U.K., Physical and Theoretical Chemistry, University of Oxford, Parks Rd South, Oxford, OX1 3QZ, U.K., Institut Laue Langevin, 6 rue Jules Horowitz, Grenoble Cedex 9, 38042 France, and National Institute for Science and Technology Center for Neutron Research, 100 Bureau Drive, Gaithersburg, Maryland

Received April 22, 2008. Revised Manuscript Received June 6, 2008

The impact of the nonionic surfactant, dodecyl triethyleneglycol ether ($C_{12}E_3$) on the solution microstructure of the dialkyl chain cationic surfactant, dihexadecyl dimethyl ammonium bromide, (DHDAB) has been investigated. The variation in solution microstructure has been studied using a combination of small angle neutron scattering, ultra small angle neutron scattering, optical texture and photon correlation spectroscopy. At low surfactant concentrations (1.5 mM) the microstructure takes the form of bilamellar vesicles (BLV) for compositions containing less than 20 mol % of added $C_{12}E_3$. Multilamellar vesicles (MLV) are the predominant microstructure for solutions richer in composition than 20 mol % $C_{12}E_3$. At more than 80 mol % $C_{12}E_3$, the solution microstructure reverts to that of a lamellar phase dispersion consistent with studies on the pure nonionic surfactant. At higher concentrations (60 mM) a wide continuous L_β phase region is observed for compositions in the range 20 to 80 mol % $C_{12}E_3$. The fine details of the phase diagram were obtained from quantitative analysis of the SANS data using a well-established lamellar membrane model. Irrespective of the nonionic content, the bilayers are in general highly rigid, consistent with those stabilized by charge interactions. Furthermore estimates of the product of membrane moduli (compressibility and bending modulus) indicate that the different phase regions have very different membrane properties, however the magnitude of the variations observed are not predicted using existing theoretical treatments.

1. Introduction

Surfactant mixtures are important in many applications such as consumer products, (detergents, shampoos and conditioners) and in lubricants. The mixing of different types of surfactants provides synergies which optimize detergency, flow characteristics and/or colloidal stability. Consequently surfactant mixing has been extensively studied, both theoretically and experimentally,[1,2] and many aspects are now relatively well understood. However, there are still areas which are poorly understood or relatively unexplored, especially in cases where significant departure from ideal mixing is observed.

Particularly important in lubricants but also a major constituent of both hair and clothes care products, are the dialkyl chain cationic surfactants. Largely due to their low solubility, they are usually formulated in conjunction with other surfactants/cosurfactants, particularly polyoxyethylene glycol nonionic surfactants.[3] Furthermore there is an emerging parallel with biomembranes, where the main ingredients are dialkyl chain lipids, and in membrane solubilization studies.[4] Although there is a relatively rich literature on the phase behavior of the dialkyl chain cationic surfactants[5–9] there is, by comparison, relatively little literature concerning the phase behavior of dialkyl chain cationic/nonionic surfactant mixtures and almost nothing on their associated surface adsorption behavior.[10,11]

Dialkyl chain cationic surfactants have a low or zero spontaneous curvature, and will predominantly self-assemble into planar structures; that is, lamellar or vesicular aggregates. For alkyl chain lengths greater than C_{12} the lamellae which form at room temperature consist of bilayers whose central core (the alkyl chain region) is a frozen structure, that is an L_β phase. In contrast, the polyoxyethylene glycol nonionic surfactants (C_nE_m) can have a range of spontaneous curvatures, from planar to highly curved micellar structures, depending upon the ethylene oxide chain length and the alkyl to ethylene oxide chain length.[12] For instance if *n* is 12 and *m* is 3, the predominant form of the bulk aggregate is a bilayer with a fluid core, and the associated lamellar phase is in the L_α phase.

The motivation for the current study was to investigate how mixing a nonionic with low spontaneous curvature, but which form a fluid bilayer (that is, the L_α phase), would affect the bulk solution behavior of the L_β phase forming surfactant dihexadecyl

* To whom correspondence should be addressed. E-mail: ian.tucker@unilever.com.
† Unilever Research and Development Port Sunlight.
‡ STFC Rutherford Appleton Laboratory.
§ University of Oxford.
|| Institut Laue Langevin.
⊥ National Institute for Science and Technology Center for Neutron Research.

(1) Scamehorn, J. F., *in 'Mixed surfactant systems'*, Eds, Ogino, K Abe, M Marcel Dekker, NY 1997.
(2) Holland, P. M., Rubingh, D. N. *in 'Cationic surfactants'*, Eds P. M. Holland, D. N. Rubingh, Surfactant Science Series, 1990 *vol 37*, Marcel Dekker, NY.
(3) Penfold, J.; et al. *J. Phys. Chem. B* **2005**, *109*, 18107.
(4) Almgren, M. *Biochem. Biophys. Acta* **2000**, *1508*, 146.
(5) Dubois, M.; Zemb, T. *Langmuir* **1991**, *7*, 1357.
(6) Zemb, T.; Gazeau, D.; Dubois, M.; Gulik-Krnywicki, T. *Euro. Phys. Lett.* **1993**, *21*, 759.
(7) Haas, S.; Hoffmann, H.; Thunig, C.; Hoinkis, I. E. *Colloid Polym. Sci.* **1999**, *277*, 856.
(8) Brady, J. E.; Evans, D. F.; Warr, G. G.; Grieser, F.; Ninham, B. W. *J. Phys. Chem.* **1986**, *90*, 1853.
(9) Cabois, F.; Moduzzi, M. *Langmuir* **1996**, *12*, 3548.
(10) Junquera, E.; del Burgo, P.; Arranz, R.; Llorca, O.; Aicart, E. *Langmuir* **2005**, *21*, 1795.
(11) Penfold, J.; Staples, E.; Tucker, I.; Thomas, R. K. *Langmuir* **2004**, *20*, 1269.
(12) Mitchell, D. J.; Tiddy, G. J. T.; Waring, L.; Bostock, T.; Macdonald, M. P. *J. Chem. Soc., Faraday Trans. I* **1983**, *79*, 975.

10.1021/la8012359 CCC: $40.75
Published on Web 08/15/2008

dimethyl ammonium bromide, (DHDAB). This work is part of a broader study concerning the surface and solution properties of DHDAB alone and in mixtures with a range of different nonionic cosurfactants,.[3,11,13–15] Measurements were made over a range of compositions, from cationic to nonionic rich, and for a range of concentrations, from dilute to concentrated solutions. The phase behavior was determined largely using small angle neutron scattering, SANS, ultrasmall angle scattering, USANS, optical texture measurements, and dynamic light scattering, PCS. Complementary measurements on the solution behavior of DHDAB, DHDAB/$C_{12}E_6$ and DHDAB/$C_{12}E_{12}$ mixtures are reported elsewhere.[14,15] In the context of the range of applications of such mixtures the adsorption behavior is crucially important, and the interplay between the adsorption behavior and the associated evolution in the solution microstructure are also reported separately.[15]

2. Experimental Details

Small angle neutron scattering, SANS, was the main measurement technique used to probe the solution microstructure. It was complemented by the visual assessment of solution optical texture, and PCS measurements. Additional complementary USANS measurements were made to reinforce the SANS, PCS and optical data, where needed to impart further clarity.

2.1. Materials and Measurements Made. For the dilute solutions, (1.5 mM), SANS measurements were made for DHDAB/$C_{12}E_3$, mixtures for solution compositions ranging from 100:0 to 0:100 at 10% intervals in composition. Further SANS measurements were made at higher surfactant concentrations, in the range 10 to 160 mM, over the entire composition range at compositions either within or close to phase boundaries. All solutions for SANS were prepared in D_2O (Fluorochem), at 5 mL scale, heating to 60 °C and then maintaining the solutions above 30 °C to maintain the solutions above the Krafft point of DHDAB. (This method, adopted for producing solutions of DHDAB (and mixtures with nonionic surfactants) with high reproducibility is described in more detail in refs 13 and 14). Samples were transferred to 1 mm path length Starna quartz spectrophotometer cells for the SANS measurements. The cells were cleaned in Decon 90 and rinsed in pure water (Elga Ultrapure). All the samples were measured at 30 ± 1 °C. The h-DHDAB was obtained from Fluka and was recrystallized from ethyl acetate. Hydrogenous $C_{12}E_3$ was obtained from Nikko Chemicals Japan, and was used as supplied.

2.2. Small Angle Neutron Scattering, SANS. SANS measurements on dilute solutions (1.5 mM) were made on the D22 diffractometer at the ILL, France.[16] Measurements at higher surfactant concentrations (>10 mM) were made on both the D22 and D11 diffractometers at the ILL, France,[16] and on the LOQ diffractometer at ISIS, UK.[17] On D22 the measurements were made at a neutron wavelength, λ, of 8 Å, and a $\triangle\lambda/\lambda$ of 10%, and two sample to detector distances, 3.5 and 16.5 m, to cover a scattering vector, Q, range of 0.002 to 0.2 Å^{-1} (where the scattering vector, Q, is defined as $Q = 4\pi/\lambda \sin(\theta/2)$, and θ is the scattering angle). The D11 measurements were made at a neutron wavelength, λ, of 6 Å, and a $\triangle\lambda/\lambda$ of 10%, and three sample to detector distances, 1.1, 5.0 and 16.5 m, to cover a scattering vector, Q, range of 0.003 to 0.25 Å^{-1}. On LOQ the measurements were made using the white beam time-of-flight method, using neutron wavelengths in the range 2 to 10 Å, and a sample to detector distance of 4 m, to cover a Q range of 0.008 to 0.25 Å^{-1}. All the measurements were made in D_2O, with an 8 mm diameter beam, and the solutions were contained in 1 mm path length Starna quartz spectrophotometer cells. All the solutions were measured at 30 ± 1 °C. The data were corrected for background scatter, detector response, spectral distribution of the incident beam (for LOQ) and converted to an absolute scattering cross section, $d\sigma/d\Omega$, (in cm^{-1}), using standard procedures.[18,19]

2.3. USANS. Some USANS measurements were made on a limited subset of samples using the Bonse-Hart double crystal diffractometer, BT5, at NIST.[20] Those measurements extended the Q range accessible to 5×10^{-5} Å^{-1} (5×10^{-5} to 5×10^{-3} Å^{-1}) to provide an estimate of the overall size of the predominantly cationic rich planar structures (lamellar fragments, vesicles). Because of the slit geometry the data were desmeared and normalized using standard procedures.[21]

2.4. Photon Correlation Spectroscopy (PCS). Dynamic light scattering measurements, PCS, were made using a Malvern PCS8 instrument upgraded to a 7132A correlator, and version 1.41b of the software. Laser light at 300 mW and wavelength 488 nm was provided using a Lexel M85 water cooled Ar^+ ion laser. Data were collected in triplicate, where each measurement lasted for 120s. The resultant autocorrelation functions were analyzed using the Contin method to obtain the particle size and size distribution (where σ = one standard deviation).[22] These measurements provided an additional and important independent estimate of the overall size of the cationic rich microstructures (lamellar fragments, vesicles). All experiments were performed at a temperature of 30 ± 0.1 °C.

2.5. Optical Texture Measurements. Following a similar approach to that of Dubois et al.,[5] optical texture measurements were made using both polarized and unpolarised white light, and were used to provide an initial qualitative evaluation of the solution phase behavior.

2.6. SANS Data Analysis. The form of the SANS scattering patterns (Q dependence) was used qualitatively to identify the lamellar (vesicular), micellar, and mixed phase regions of the overall phase behavior. As the nature of the SANS data were mostly consistent with multilamellar vesicles, the data were predominantly quantitatively analyzed using an implementation of the Nallet lamellar scattering model.[23] The scattering pattern is analyzed to estimate the Caille parameter, η, (which is related to lamellar membrane rigidity and compression modulus), the number of layers/lamellae, N, the bilayer spacing, d, and the thickness of the bilayer, δ. An analytical expression for $d\sigma/d\Omega$ takes into account the lamellar form factor, $P(Q)$, and the structure factor, $S(Q)$, taking into account membrane fluctuations, the contribution of resolution to the line width, and assuming a powder average, such that

$$\frac{d\sigma}{d\Omega} = 2\pi\frac{V}{d}\frac{1}{Q^2}P(Q)\,\bar{S}(Q) \tag{1}$$

where V is the irradiated volume, and $P(Q)$ and $S(Q)$ are given by

$$P(Q)\frac{4}{Q^2}\Delta\rho^2 \sin^2\left(Q\frac{\delta}{2}\right) \tag{2}$$

$$\bar{S}(Q) = 1 + 2\sum_{1}^{N-1}\left(1-\frac{n}{N}\right)\cos\left(\frac{Qdn}{1+2\sigma_Q d^2\alpha(n)}\right)e - \frac{2Q^2d^2\alpha(n)+\sigma_Q d^2 n^2}{2(1+2\sigma_Q d^2\alpha(n))}\frac{1}{\sqrt{1+2\sigma_Q d^2\alpha(n)}} \tag{3}$$

where for small n

(13) Tucker, I. M., *D.Phil. Thesis*, University of Oxford, (2007).
(14) Tucker, I., Penfold, J. , Thomas, R. K. , Grillo, I., Mildner, D., Barker, J. G., *Langmuir* 2008. web alerts DOI: 10.1021/la703415m.
(15) Tucker, I., Penfold, J., Thomas, R. K., Grillo, I., Mildner, D. , Barker, J. G., *Langmuir* 2008. in preparation.
(16) Neutron beam facilities at the high flux reactor available for users', ILL, Grenoble, France 1994.
(17) Heenan, R. K.; King, S. M.; Penfold, J. *J. Appl. Crystallogr.* **1997**, *30*, 1140.
(18) Ghosh, R. E., Egelhaaf, S. U., Rennie, A. R., *ILL Int Rep* 1998 ILL98GH14T.
(19) Heenan, R. K., King, S. M., Osborn, R., Stanley, H. B, *RAL Int Rep* 1989RAL-89−128.
(20) Barker, J. G.; Glinka, C. J.; Moyer, J. J.; Kim, M H.; Drews, A. R.; Agamalian, M. *J. Appl. Crystallogr.* **2005**, *38*, 1004.
(21) Lake, J A. *Acta Crystallogr.* **1967**, *23*, 191.
(22) Provencher, S. W. *Makromol Chem* **1979**, *180*, 201.
(23) Nallet, F.; Laversanne, R.; Roux, D. *J. Phys II France* **1993**, *3*, 487.

$$\langle (u_n - u_0)^2 \rangle = \frac{\eta n^2 d^2}{8} \quad (4)$$

and $\alpha(n)$ is the correlation function given by

$$\alpha(n) = \langle (u_n - u_0)^2 \rangle / 2d^2 \quad (5)$$

η is the Caille parameter, which is related to the membrane moduli

$$\eta = \frac{Q_0^2 k_B T}{8\pi\sqrt{KB}} \quad (6)$$

where B is the compression modulus and K the bending modulus. σ_Q is shorthand for $\Delta Q/Q$, the instrumental resolution,[24] and $Q_0 = 2\pi/d$.

For the USANS data, a core + shell model was used[25] where

$$\frac{d\sigma}{d\Omega} = nS(Q)|\langle F(Q)\rangle_Q|^2 + \langle |F(Q)|^2 \rangle_Q - |\langle F(Q)\rangle_Q|^2 \quad (7)$$

where the averages denoted by $\langle Q \rangle$ are averages over particles size and orientation, n is the aggregate number density, $S(Q)$ the interparticle structure factor, and $F(Q)$ the particle form factor. The particle structure (form factor, $F(Q)$) is modeled using a standard 'core and shell' model,[25] where the form factor is

$$F(Q) = V_1(\rho_1 - \rho_2)F_0(QR_1) + V_2(\rho_2 - \rho_s)F_0(QR_2) \quad (8)$$

and R1, R2 are the core and shell radii, $V_i = 4\pi R_i^3/3$, $F_0(QR_i) = 3j_1(QR_i)/(QR) = 3[\sin(QR) - QR\cos(QR)]/(QR)^3$, ρ_1, ρ_2 and ρ_s are the scattering length densities of the particle core and shell, and of the solvent, and $j_1(QR_i)$ is a first order spherical Bessel function. The 'decoupling approximation' assumes that for interacting (finite $S(Q)$) pseudo spherical particles there is no correlation between position, size and orientation. The structure factor, which quantifies the interparticle interactions/correlations, is included using the RMSA calculation[26,27] for a repulsive screened Coulombic interaction potential, characterized by the surface charge of the vesicle, z, the Debye−Huckel inverse screening length, K_{DH} (defined in the usual way), and the particle number density, n. In this instance the form factor, $F(Q)$, is a core−shell model constrained to space fill with an inner core corresponding to that of the solvent and the outer shell that of the vesicle bilayer or multilayer. The data were consequently expressed as a diameter with a tolerance, σ, equal to one standard deviation.

3. Results

The variation in solution optical appearance with temperature is shown in Figure 1.

There was no evidence of optical rotation which normally indicate the existence of large asymmetric objects, for example, lamellar phase regions. The changes in solution appearance suggest that three separate phase regions exist at 1.5 mM. The first spanning 100:0 to 50:50 compositions, the second up to 30:70 composition and the third where the solutions contained the highest nonionic compositions (>80 mol % $C_{12}E_3$). The patterns recorded at low temperature, were reproduced following cooling from 70 °C, and the variation of optical texture with temperature served to pinpoint the location of the transition to the known L_α phase in the nonionic rich samples.[28] The absence of optical rotation in the DHDAB rich region renders a more detailed phase assignment (and explanation of the variation in optical texture) impossible and justifies the use of SANS.

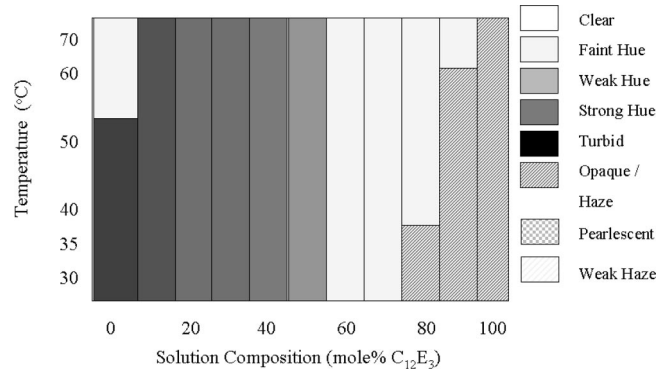

Figure 1. Variation in optical texture of DHDAB $C_{12}E_3$ mixtures with composition and temperature.

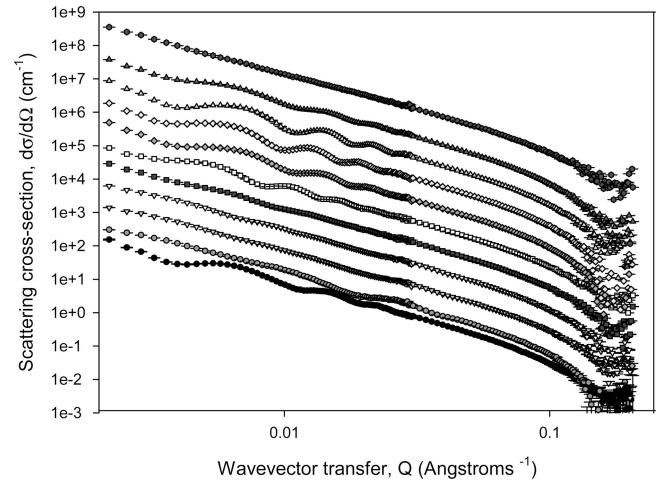

Figure 2. Combined SANS scattering data for 1.5 mM DHDAB $C_{12}E_3$ mixtures at mole ratios of 100:0 (black diamond),90:10 (red circles), 80:20 (green triangle), 70:30 (yellow triangle), 60:40 (blue square), 50:50 (white square), 40:60 (pink diamond), 30:70 (cyan diamond), 20:80 (gray triangle), 10:90 (olive triangle) and 100:0 (purple circle). The scattering data are each displaced by a multiple of 4 to avoid overlay with the 100:0 shown on the absolute scale. The errors are smaller than the data points used in the figure.

Figure 2 shows the corresponding SANS data measured at 30 °C for 1.5 mM solutions of composition varying from 100:0 mol % DHDAB:$C_{12}E_3$ to 0:100 composition at 10 mol % intervals.

The SANS data are consistent with the scattering from planar objects, where the general form of the scattering has a Q^{-2} dependence. By analogy with previous work on the pure DHDAB system,[14] attempts were made to model the intensity modulations on the scattering as vesicles using a core + shell unilamellar vesicle model with low polydispersity. It was not possible to accurately fit all of the undulations, nor was it possible to achieve an adequate damping of the oscillations without applying an unphysically large polydispsersity (>50%). PCS data were measured but it was difficult to fit the autocorrelation functions obtained to particle size distributions because of their extreme polydispsersity, and the complex nature of the particle size distributions was later confirmed by analysis of USANS measurements (see later).

Plotting the scattering data as IQ^2 vs Q renders the lamellar features in the scattering more visible and suggests that the intensity modulations were a consequence of lamellar ordering,

(24) Grillo, I. , ILL Technical Report 2001 ILL01GR08T.
(25) Hayter, J. B.; Penfold, J. *Colloid Polym. Sci.* **1983**, *261*, 1072.
(26) Hayter, J. B.; Hansen, J. P. *Mol. Phys.* **1982**, *42*, 651.
(27) Hayter, J. B.; Penfold, J. *Mol. Phys.* **1981**, *42*, 109.
(28) Laughlin, R. G.; Lynch, M. L.; Marcott, C.; Munyon, R. L.; Marrer, A. M.; Kochvar, K. A. *J. Phys. Chem. B* **2000**, *104*, 7354.

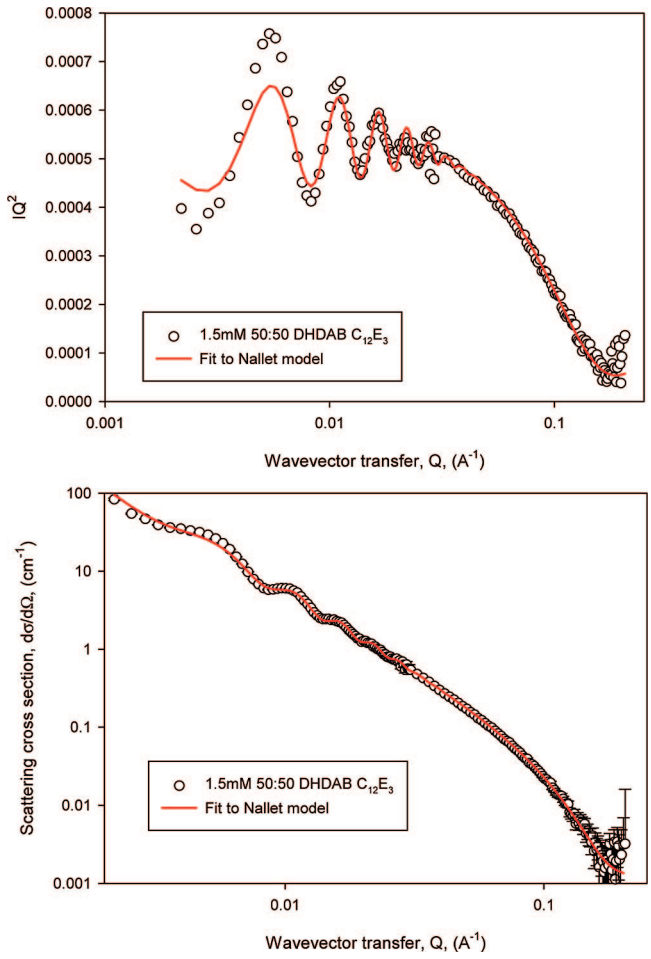

Figure 3. Fit to the scattering from 1.5 mM 50:50 DHDAB $C_{12}E_3/D_2O$ at 30 °C using the Nallet model. (a) Data displayed as IQ^2 vs Q to amplify the appropriate features of the scattering, (b) displayed as conventional I vs Q.

consistent with a similar behavior observed for pure DHDAB.[14] Figure 3 shows some typical data plotted both conventionally ($I(Q)$ vs Q) and as $I(Q)Q^2$ vs Q, together with the fit to the Nallet lamellar phase model.

As shown in Figure 3, applying the Nallet model resulted in very good fits to the data, and an example of a typical fit to scattering data (in this case for 1.5 mM 50:50 DHDAB $C_{12}E_3$ in D_2O). The data show a minor mismatch at low Q in the region of the first order Bragg peak, whereas the Nallet model fit to the rest of the scattering data is excellent. The discrepancy in the fit at low Q is due to the form of the resolution function used, an aspect discussed in detail elsewhere.[13,14] Data for 100% DHDAB and the composition range 90:10 to 30:70 mol % DHDAB $C_{12}E_3$ were well fitted by the Nallet multilamellar model, and the key parameters derived from the fits are shown in Table 1. Compositions richer in nonionic than and including 20:80 could not be adequately fitted by the Nallet model.

The data at the DHDAB rich end of the composition range are bilamellar vesicles whose radii are sufficiently large and polydisperse that their form factor has little or no effect on the SANS data (over the Q-range probed). As the solution composition becomes richer in $C_{12}E_3$, N, the number of layers, in general increases and at 20 mol % nonionic and above, the solution microstructure is now consistent with multilamellar vesicles. Further increases in nonionic content in general result in increases in lamellar d-spacing and in the number of layers. Between 50:50 and 30:70 the interlayer spacings are consistently larger than the DHDAB rich counterparts, coincident with the region of reduced optical texture in Figure 1. In this region both N and the d-spacing have substantially increased, with consequential increase in vesicle size, and this is responsible for the significant differences in optical texture. The Caille parameters derived from the fits show very little variation and are relatively small, implying that the lamellae are highly rigid consistent with those stabilized by charge interactions. Contrary to expectations, incorporation of $C_{12}E_3$ into the bilayer does not make the lamellae more fluid-like. The data corresponding to 20:80 to 0:100 mole ratio DHDAB $C_{12}E_3$ cannot be fitted to the Nallet model. This, together with the visual observations (Figure 1), is consistent with a change of bulk aggregate structure in this region of the phase diagram.

Table 1. Model Fits to the Nallet Model for DHDAB $C_{12}E_3$ Dispersions in D_2O at 30 °C[a]

composition DHDAB:$C_{12}E_3$	layer spacing, $d \pm 5$(Å)	layer thickness, $\delta \pm 0.2$(Å)	Caille parameter, $\eta \pm 0.003$	number of layers, $N \pm 1$
100:0	850	33.7	0.07	2
90:10	875	34.7	0.07	2
80:20	875	34.1	0.05	8
70:30	980	31.4	0.05	14
60:40	905	31.6	0.06	2
50:50	1160	32.7	0.03	41
40:60	1030	34	0.10	2
30:70	1455	31	0.05	12

[a] The error, σ, is 1 standard deviation.

In related work concerning the surface properties of these and other DHDAB nonionic mixtures,[15] a maximum in the mixed CAC variation with composition observed at 80:20 mole ratio in DHDAB $C_{12}E_3$ mixtures. This maximum, characteristic of phase separation/demixing, coincides with the transition from bilamellar to multilamellar vesicles in the current study. There is a corresponding reduction in bilayer thickness, δ, from 34 to 31 Å between 80:20 and 70:30 compositions and this suggests that it is a reorganization of the internal structure of the bilayer that drives the phase transition (and which is also responsible for the release of nonionic monomer at solution compositions richer in nonionic than 80:20[15]). Further detail about the microstructure evolution at 80:20 composition was obtained from analysis of the USANS data.

Figure 4a shows the desmeared data obtained for 1.5 mM 80:20 DHDAB $C_{12}E_3$, and Figure 4b the data corresponding to 20:80 composition. These data show that the maximum aggregate dimension at 80:20 composition is much larger than the 2800 Å ($\sigma = 0.48$), previously obtained for 100% DHDAB at the same concentration,[14] and as the lamellar d-spacings are similar to those obtained for 100% DHDAB this suggests a multilamellar rather than bilamellar format for the vesicles. Furthermore there are two inflection points in the desmeared data, which are also present in the nondesmeared raw data. It was not possible to model the data using a single particle size distribtution and the two curves in Figure 4a represent attempts to model this data using a bimodal distribution based on the polydisperse core + shell model. The parameters used to constrain the model for both data are listed in Table 2. It suggests that at the 80:20 composition two very polydisperse but discrete particle size distributions exist, with large particles of the order of 18000 Å ($\sigma = 0.88$), coexisting with a smaller particle of approximately 800 Å ($\sigma = 0.63$). A consequence of parameters from the Nallet analysis of the SANS data is that the aggregates are micrometer-sized. Hence it is clear that the SANS data are being dominated by the scattering from the multilamellar vesicles. Data obtained for the 20:80 samples are shown in Figure 4b together with the fit to the same model.

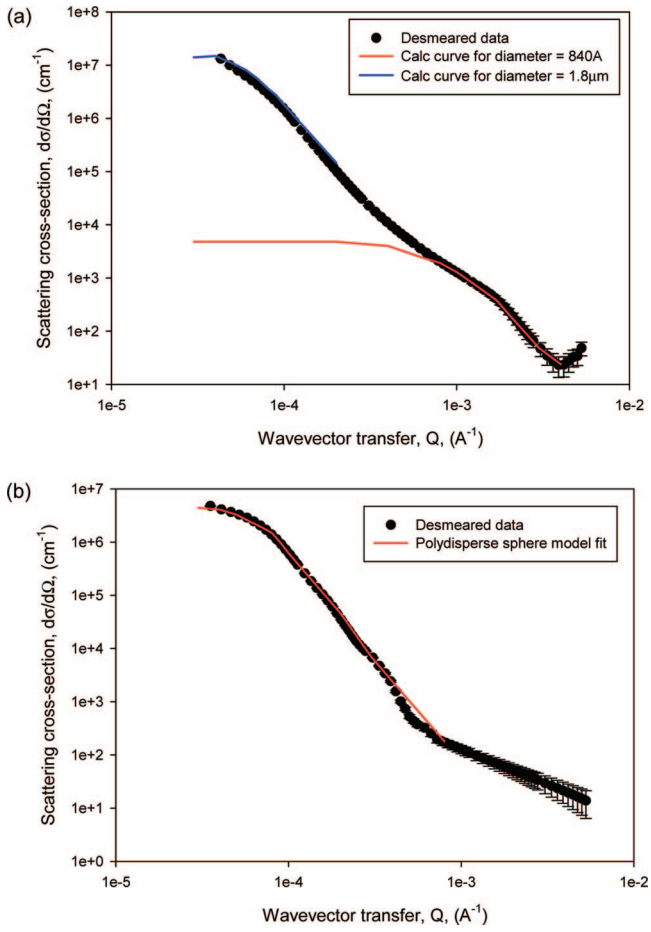

Figure 4. USANS data for 1.5 mM DHDAB $C_{12}E_3$ mixtures at 30 °C: (a) 80:20 composition; (b) 20:80 composition.

Table 2. Parameters Used in the Core + Shell Model for USANS Analysis of 1.5 mM DHDAB $C_{12}E_3$ Mixtures

	80:20 large size	80:20 small size	20:80
core radius (Å), R_2	9000 ± 50 Å	400 ± 20 Å	5500 ± 50 Å
polydispersity, σ	0.89 ± 0.02	0.63 ± 0.02	0.82 ± 0.02
phase volume, ϕ	0.0025 ± 0.0001	0.0015 ± 0.0001	0.0011 ± 0.0001
layer thickness, $(R_2 - R_1)$	28 ± 0.2	29 ± 0.2	32 ± 0.2
$1/\kappa$	0.1 ± 0.01	0.1 ± 0.01	0.1 ± 0.01
Z (electronic charge)	0.02 ± 0.001	0.02 ± 0.001	0.02 ± 0.001

The fits obtained for the 20:80 are consistent with a single particle size distribution of 11000 Å ($\sigma = 0.82$).

Additional evidence for the coexistence of two aggregate forms was obtained from visual observation of the sample following an extended period of storage. Figure 3 in the Supporting material shows that following a period of 22 months at 30 °C, there is evidence of physical phase separation. However this was only observed for the 80 and 60 mM samples at 80:20 composition.

In order to obtain a more complete picture of the phase behavior evolution, further data were collected at higher solution concentrations for different compositions close to or well within predicted phase boundaries. Scattering data from more concentrated samples at mole ratios of 80:20 50:50, 20:80 and 0:100 were collected on the LOQ diffractometer. These were complemented by further data collected on the D11 diffractometer at the ILL at concentrations of 10, 20 and 60 mM and compositions of 80:20 60:40 and 40:60 cationic nonionic. The 2-D patterns corresponding to the 80 mM solution concentration, representative of the data obtained, are shown in Figure 5.

In common with the scattering from pure DHDAB, the scattering is isotropic throughout the concentration and composition range measured, indicating that the scattering originates either from objects which possess three-dimensional symmetry or that the particles are sufficiently small or dilute such that the scattering is rotationally averaged. PCS had again indicated particle sizes of 200−300 nm, lending support to the initial hypothesis, that the particles are rotationally symmetrical. As the 2-D scattering patterns gave no indication of preferred orientation the data obtained from each of the four compositions discussed above were radially averaged and the data for each composition series are presented as scattering cross section, $d\sigma/d\Omega$ versus wavevector transfer, Q, in Figure 6.

The radial averaged scattering patterns from 80:20 mol % DHDAB $C_{12}E_3$ mixtures are shown in Figure 6a. An underlying Q^{-2} dependence at all concentrations is consistent with the existence of planar structures. In addition structural features appear at higher solution concentrations in the form of distinct Bragg peaks. At the highest concentration these are absent, indicating a further change in bulk mesophase. Although at the temperature measured the solution is in the L_β condition for pure DHDAB, the addition of $C_{12}E_3$ to this system now introduces the possibility of membrane undulations as, at 30 °C, $C_{12}E_3$ lamellar phase dispersions will be in the L_α phase. Well defined Bragg peaks are visible for 80 and 120 mM DHDAB. Data obtained for 50:50 composition (Figure 6b) are mostly consistent with the 80:20 data, with perhaps some evidence of anisotropy in the scattering in the higher concentration data. The data for 20:80 molar composition (Figure 6c) also have the Q^{-2} dependence consistent with planar objects and for the two highest concentrations the Bragg peaks overlay this Q^{-2} behavior. Where Bragg peaks are observed, the peak positions move to higher Q with increasing concentration, as expected. Anisotropic scattering patterns at 120 mM and higher indicate a microstructure containing orientable domains of lamellar phase rather than BLV or MLV. Data for 0:100 molar composition, that is, 100% $C_{12}E_3$ also show the Q^{-2} dependence indicative of planar structures. The form of the data become more complex at higher concentrations and the origins of the broad Bragg peak observed are probably due to the formation of a bicontinuous/hydrated solid phase. For the 80:20 data at high concentration the fits to the data (in particular to the first Bragg peak) are now less good, which may indicate preferred orientation of the lamellar phase due to the existence of large lamellar fragments at this composition. For the 50:50 data there is a clear variation in the magnitude of the model parameters consistent with there being a phase boundary at this composition. To obtain a more quantitative description, the data were analyzed using the Nallet model, and the results are summarized in Table 3.

Consistent with changes in the scattering behavior observed are both a significant reduction in Caille parameter (indicating a sharp increase in bilayer rigidity) and an order of magnitude increase in the number of bilayers. As these are accompanied by changes in optical texture the position of the phase boundary can be accurately located between 80 and 120 mM at 20:80 composition and to between 40 and 80 mM for 50:50 and 80:20 mole ratios of DHDAB to $C_{12}E_3$. The isotropic nature of the 2-D scattering patterns at 80 mM 50:50 and 80:20 compositions is most consistent with small lamellar domains which are not oriented during the process of filling the cell. These data were also analyzed using the Nallet approach, and the results are presented in Table 4.

Overall the two sets of data reported in Tables 3 and 4 are in reasonable agreement. It is possible to obtain more reliable model

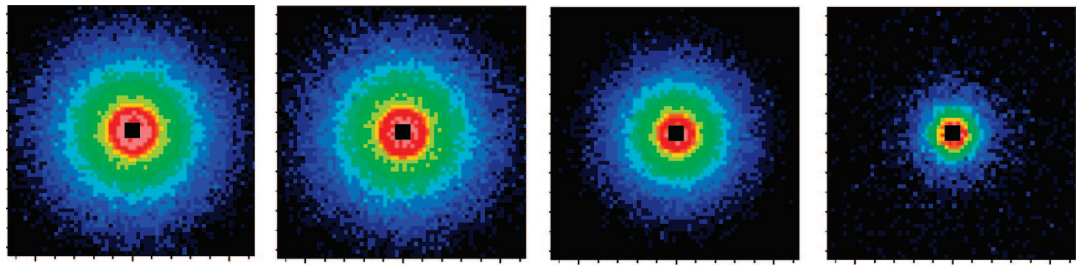

Figure 5. 2-D scattering from 80 mM DHDAB $C_{12}E_3$ at mole ratios of 80:20 50:50 20:80 and 0:100. Temperature 30 °C.

parameters from the D11 and D22 data than from LOQ because of the better resolution available on these two instruments in the *Q*-range of interest.[13,14] This is discussed in more detail in Section 2 of the Supporting Information.

The variation in optical texture with concentration and composition for DHDAB $C_{12}E_3$ is shown in figure 7.

The optical texture data, the SANS data and the details provided by the Nallet analysis of the SANS data have been used to construct a phase diagram (Figure 8). The MLV region was assigned on the basis of the value of N being >2, and MLV/continuous L_β for $N > 20$. The composition/concentration dependence of the Caille parameter was obtained from the Nallet analysis. It was observed that there is a region in the mid concentration range (40 mM 60:40 to 20:80) where the bilayers are less rigid than at low concentrations while still being BLV. These regions are assigned as BLV(1) and BLV(2) regions. Furthermore, the variations in bilayer thickness were used to confirm the position of phase boundaries. For example, the BLV/MLV boundary was located by the reduction in bilayer thickness from 34 to 31 Å. The exception was for $C_{12}E_3$ alone where the Nallet analysis was not possible and the mesophase structure assigned by inspection of the visual appearance of the samples alone. This compared well with the phase behavior for pure $C_{12}E_3$ published by Laughlin et al.[28] The resulting bulk phase diagram for DHDAB $C_{12}E_3$ derived from a combination of the optical and SANS data is shown in Figure 8. The additional detail, not usually present is a consequence of the detail obtained from the analysis of SANS data.

The microstructure is predominantly in the form of vesicles. There is some evidence that the central MLV region subdivides into a continuous lamellar at above 50 mol % nonionic for concentrations greater than 80 mM. This is based on the anisotropic nature of the 2-D scattering patterns in these static SANS measurements, and have since been confirmed with SANS measurements under shear.[29]

4. Discussion

4.1. Effect of $C_{12}E_3$ on DHDAB Bilayer Properties. It was expected that the addition of $C_{12}E_3$ would alter the bilayer properties significantly when mixed with DHDAB. At a temperature of 30 °C, solutions composed entirely of $C_{12}E_3$ are lamellar phase dispersions.[12,30] Being in the fluid L_α phase at 30 °C, $C_{12}E_3$ should have a relatively large Caille parameter (~1) consistent with those reported in systems which are stabilized purely by undulations.[31,32] On the basis of other reported work,[27,31,32] it was expected that mixing $C_{12}E_3$ with DHDAB would induce a dramatic reduction in bilayer rigidity of the DHDAB and correspondingly increase the Caille parameter to values which are intermediate between those for rigid (η typically ~0.01) and for flexible bilayers (η typically 0.5−1.0) in the midrange of compositions (say 40:60 to 60:40), reflecting the change in relative importance of electrostatics and undulations in stabilizing the bilayers,.[33] In the dilute samples (1.5 mM), the increase in the *d*-spacing induced by the introduction of >40 mol % $C_{12}E_3$ is most likely due to long-range electrostatic interactions. It would appear that rather than rendering the bilayer more fluid, an effect of $C_{12}E_3$ is to enhance the range of electrostatic interactions within the bilayer, due to replacement of cationic by nonionic surfactant in the bilayer. It is presumed that this is a consequence of reduced electrostatic screening due to a lowering of the counterion concentration in the interstitial water layer. However being further separated the lamellae ought to experience a lower repulsive field from their neighbors and as they separate the Caille parameter ought to increase as the system would be able to accommodate larger membrane fluctuations. However the invariance in Caille parameters with composition and their consistently low value is inconsistent with the lamellae becoming more fluid. Indeed the low value of the Caille parameter indicates that the lamellae are relatively rigid in the composition range 100:0 to 30:70 and that in this composition range electrostatics dominate the bilayer properties. This must reflect the importance of cosurfactant chain length and the associated hydrophobic chain contribution to the self-assembly and the bilayer bending modulus, κ, as discussed by Szleifer et al.[34] From their work, it would be expected that a shorter chain cosurfactant could give rise to a more significant change in membrane rigidity, and Hoffmann has demonstrated such a reduction in bilayer rigidity in the tetradecyl dimethylamineoxide/tetradecyl trimethylammonium bromide/*n*-hexanol system.[35] What is clear, however, is that at low solution concentrations the addition of $C_{12}E_3$ causes the lamellar *d*-spacing to increase significantly. This, together with the invariance in Caille parameter, cannot be ascribed to an increase in Hellfrich type fluctuations.[36] Instead it is assumed to be the result of long-ranged electrostatic interactions. If the $C_{12}E_3$ headgroup is laterally screening the DHDAB headgroup charges, favoring counterion dissociation, then an increase in the bilayer electrostatic repulsion would result.

The other contradiction to the original hypothesis is that $C_{12}E_3$ induces a change from bilamellar to multilamellar vesicles with thinner lamellae than those formed from DHDAB alone. This action is contrary to that observed of higher EO length ethoxylates[15] where the addition of $C_{12}E_6$ and $C_{12}E_{12}$ not only induced a competing micellar phase (and an extensive

(29) Tucker, I., Penfold, J., Thomas, R. K., unpublished data.
(30) Staples, E.; Thompson, L.; Tucker, I.; Penfold, J.; Thomas, R. K.; Lu, J. R. *Langmuir* **1993**, *9*, 1651.
(31) Roux, D.; Safinya, C. R. *J. Phys. (Paris)* **1988**, *49*, 307.
(32) Tsapis, N.; Urbach, W.; Ober, R. *Phys. Rev. E* **2001**, *63*, 041903.
(33) Yang, B. S.; Lal, J.; Richetti, P.; Marques, C. M.; Russell, W. B.; Prud'homme, R. K. *Langmuir* **2001**, *17*, 5834.
(34) Szleifer, I.; Kramer, D.; Ben-Shaul, A. *Phys. Rev. Lett.* **1988**, *60*, 1966.
(35) Bergmeier, M.; Gradzielski, M.; Hoffmann, H.; Mortensen, K. *J Phys. Chem. B* **1999**, *103*, 1605.
(36) Helfrich, W. Z. *Naturforsch* **1978**, *33a*, 305.

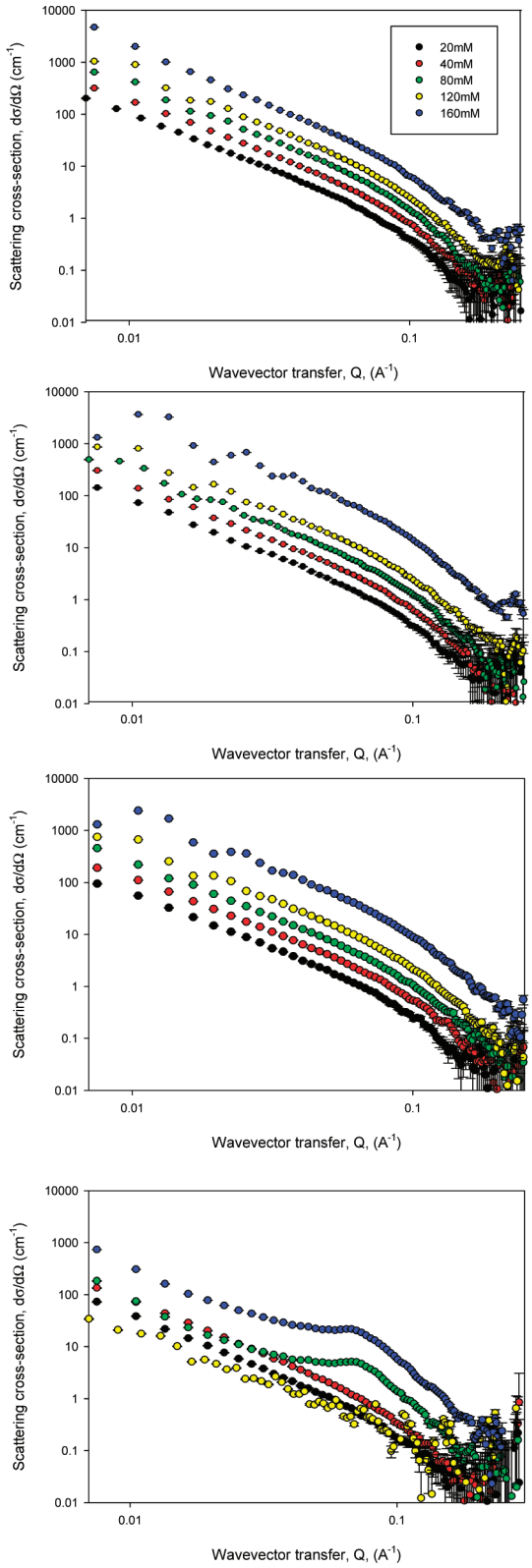

Figure 6. Intensity versus scattering vector plots for 20 mM (black), 40 mM (red),80 mM (green), 120 mM (yellow). 160 mM (blue) DHDAB $C_{12}E_3$ mixtures with varying composition: (a) 80:20 mol %, (b) 50:50, (c) 20:80 and (d) 0:100. Data are offset for clarity. The error bar is for the most part smaller than the data point.

mixed L_β/L_1 region of phase behavior) but also resulted in increased bilayer thicknesses. This is probably due to increased headgroup−solvent interactions in the higher EO length nonionics.

Table 3. Fits to the Nallet Model for Concentrated DHDAB $C_{12}E_3$ Dispersions in D_2O at 30 °C

concentration (mM), composition (mole ratio)	layer spacing, ± 5(Å)	layer thickness, ± 0.2(Å)	Caille parameter, ± 0.003	No. of layers, ± 1
20, 80:20	1360	31.8	0.62	2
40, 80:20	1780	31.8	0.10	2
80, 80:20	590	31.8	0.012	21
120, 80:20	580	33.0	0.011	39
160, 80:20	325	31.5	0.41	2
20, 50:50	530	31.8	0.31	2
40, 50:50	750	31.0	0.67	2
80, 50:50	590	33.1	0.002	33
120, 50:50	580	32.4	0.003	27
160, 50:50	490	32.1	0.004	36
40, 20:80	920	31.2	0.056	2
120, 20:80	576	30.6	0.013	39
160, 20:80	496	30.9	0.019	38

Table 4. Model Fits to the Nallet Model for DHDAB $C_{12}E_3$ Dispersions in D_2O at 30 °C, D11 Data

concentration (mM), composition (mole ratio)	layer spacing, d ± 5 (Å)	layer thickness, ± 0.2 (Å)	Caille parameter, ± 0.003	no. of layers N ± 1	phase volume, ± 0.0002
10, 80:20	655	32.9	0.02	37	0.005
20, 80:20	1000	31.3	0.01	10	0.010
60, 80:20	730	30.6	0.01	38	0.028
10, 60:40	1120	30.1	0.01	35	0.005
20, 60:40	920	30.5	0.01	48	0.010
60, 60:40	685	30.6	0.02	54	0.032
10, 40:60	1080	30.3	0.01	62	0.005
20, 40:60	930	29.7	0.01	56	0.008
60, 40:60	670	29.2	0.02	32	0.031

4.2. Membrane Rigidity. Further insight into the membrane properties can be obtained by inverting the Caille equation,[14] in terms of the membrane moduli κ and B, that is

$$\sqrt{\frac{\kappa B}{d_o}} = \frac{\pi k_B T}{2 d_o^2 \eta} \tag{9}$$

Table 5 shows the variation in the κB product calculated using eq 8 for both dilute and concentrated mixtures of DHDAB and $C_{12}E_3$. For electrostatically stabilized membranes estimates of κ and B can be obtained from the approaches of Mitchell and Ninham, [37] Richetti et al.,[38] and Roux et al.[31] The magnitude of the membrane rigidity, κ, can be estimated for ionic systems[37] as

$$\kappa = \frac{4\varepsilon_D \varepsilon_o}{\kappa_{DH}} \left(\frac{k_B T}{e}\right) \tag{10}$$

where e is the electronic charge, ε_D is the dielectric constant of water, ε_o is the permittivity of free space, κ_{DH} is the inverse Debye−Huckel screening length. For an ionic strength of 1.5 mM, $1/\kappa_{DH} \sim 100$ Å, and κ is approximately $1.5 k_B T$. Similarly assuming that the compressibility is dominated by electrostatics, B may be estimated by[38]

$$B = \frac{\pi^2 d k_B T}{2L(d-\delta)^3}\left[1 - 3\frac{\Sigma}{\alpha L(d-\delta)} + 6\frac{\Sigma^2}{\alpha^2 L^2 (d-\delta)^2} + \ldots\right] \tag{11}$$

where α is a dissociation constant (assumed to be ∼1.0), Σ is the surface area of the molecule (assumed 60 Å^2) and L is a characteristic length given by

$$L = \frac{\pi e^2}{\varepsilon_D k_B T} \tag{12}$$

and is typically ∼20 Å. For d varying from 370 to 850 Å, B varies from 13.1×10^4 ergs cm^{-3} to 1.6×10^4 ergs cm^{-3}. Included

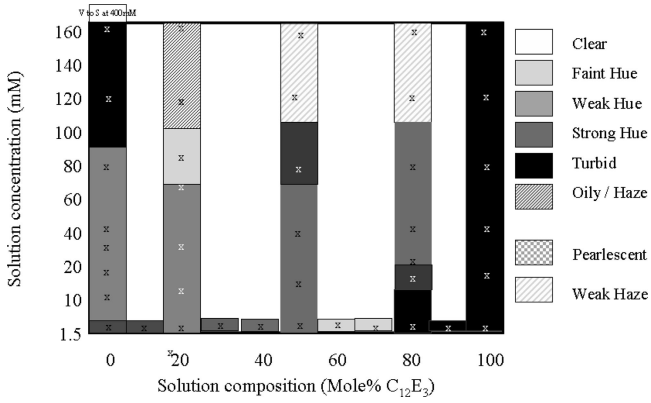

Figure 7. The variation in optical texture with concentration and composition for 1−160 mM mxitures of DHDAB $C_{12}E_3$ at 30 °C.

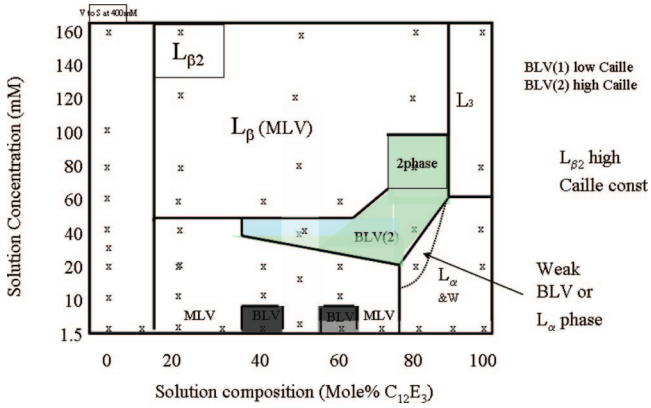

Figure 8. Phase diagram for DHDAB $C_{12}E_3$ at 30 °C. Each × represents a point on the composition concentration axes where a measurement was made.

in Table 5 are estimates of κ. B and the κB product based on eqs 10 and 11.

At 1.5 mM there is no significant change in bilayer rigidity, κB, with increasing nonionic content, despite the transition from a BLV into a MLV region. The only concentration at which there is a noticeable reduction in κB is at 30:70 composition which is close to the nonionic dominated phase boundary. Theoretical estimates of B and κ at 1.5 mM show that the absence of any strong dependence in the experimentally derived κB product can be explained by approximately equal increases and reductions in B and κ, respectively. However the decrease in κB at 40:60 composition and the absolute magnitude of the κB product are not reproduced from theory. It is now possible that as the lamellae become more $C_{12}E_3$ rich then either the effect of the hydrocarbon chain length mismatch become more important. Undulation forces are unlikely as at 30 mol % cationic, the membrane still possesses significant charge. At higher concentrations neither the magnitude nor the trend in κB product are predicted by existing theory. What is evident however is that there are significant differences in κB product in different regions of the composition/concentration axes and that these are coincident with changes in the bulk solution microstructure. In particular, the value of κB increases by more than 100 fold on changing to a continuous lamellar phase from BLV at a concentration of 60 mM. There is a transition at 160 mM 80:20 composition which coincides with the formation of a second L_β phase, as indicated on the phase diagram in Figure 8. At low concentrations there is a decrease in κB by a factor of 10 at 40:60 and 30:70 compositions. Whereas this lowering in modulus is not sufficient to induce a thermodynamically driven change in microstructure, it might make the solution more susceptible to the effects of processing and consequently the formation of multilayer vesicles.[39]

Close to the transition into a different mesophase, but still in the MLV region at 40:60, there is an order of magnitude decrease in κB. At higher solution concentrations, the change in κB is more dramatic and the variations are coincident with the regions of the phase diagram. Although it was anticipated that $C_{12}E_3$ would alter the bilayer properties, it was expected to dramatically lessen the bilayer rigidity and hence result in an increase of the Caille parameter. In fact, in terms of the κB product, the addition of $C_{12}E_3$ appears to exert very little effect on the bilayer properties at low concentration. However it does stiffen the membranes at high concentrations. Phase transitions result in significant changes in κB, suggesting an innate desire for the nonionic to disassociate from the dichain cationic surfactant. Although hydrophobic interactions would compel the surfactants to mix, the chain length mis-match between the C_{12} and C_{16} chains is the likely cause of the repulsive interactions sometimes physically manifested. According to Nagarjan,[40] a 4 hydrocarbon chain length difference corresponds to a difference in association energy of some $6k_BT$. This has not been accounted for but may well be responsible for the differences in magnitude between observed and calculated κB values, and also the origins of the physical demixing observed for 80 and 60 mM 80:20 compositions.

It is clear from the variations presented in the calculated values for κ and B that both the individual lamella properties and that of the ensemble are varying continuously. The data in Table 5 have been mapped onto the phase diagram, based on the relative magnitudes of the κB product, and this is shown in Figure 9.

In general there is very good agreement between the conventional phase diagram derived from SANS and optical texture as shown in Figure 8 and that derived from the κB product (Figure 9). As discussed previously the occurrence of the continuous L_β region is consistent with a dramatic increase in κB. The relative magnitudes of κB product in the pure DHDAB BLV and mixed MLV regions are similar, and it is only at the $C_{12}E_3$ rich end of the composition range that κB reduces significantly. The second BLV region at intermediate concentrations in the $C_{12}E_3$ rich end of the diagram is predicted, but may be narrower than assumed from Figure 8.

4.3. Phase Behavior. At the extremes of composition, that is either close to 100 mol % DHDAB or 100 mol % $C_{12}E_3$, the pure component phase behavior dominates the behavior of the mixed phases which form. From 100 mol % DHDAB to 80:20 composition, the format of the aggregates are bilamellar vesicles. At 1.5 mM the bulk behavior changes from BLV to MLV at 80 mol % composition and this coincides with changes in solution optical texture. Furthermore the bilayer thickness decreases from around 34 to 31 Å in this region of the phase diagram. This represents a reorganization of the $C_{12}E_3$ structure within the bilayer. Physical demixing in solution is evident following prolonged (2 years) storage and only at the higher solution concentrations. This suggests that at 80:20 BLV and MLV structures coexist. This is further confirmed by the analysis of USANS data at this composition.

The variations in phase behavior in DHDAB $C_{12}E_3$ are rather subtle. Similar variations have been observed in other related systems. Blom and Warr,[41] considered the interaction of both

(37) Mitchell, D. J.; Ninham, D. W. *Langmuir* **1989**, *5*, 1121.
(38) Richetti, P.; Kekicheff, P.; Parker, J. L.; Ninham, D. W. *Nature* **1990**, *346*, 252.
(39) Soubiran, L.; Staples, E.; Tucker, I.; Penfold, J.; Creeth, A. *Langmuir* **2001**, *17*, 7988.
(40) Nagarajan, R.; Ruckenstein, E. *Langmuir* **1991**, *7*, 2934.

Table 5. Summary of Bilayer Rigidity Calculations for DHDAB $C_{12}E_3$ Mixtures

concentration (mM), composition (mole ratio)	bilayer thickness, $\delta \pm 0.2$ (Å)	experimental $\kappa B \times 10^{-9}$ (ergs^2 cm^{-3})	calculated κ (k_BT)	calculated $B \times 10^4$ ergs cm^{-3}	calculated $\kappa B \times 10^{-9}$ (ergs^2 cm^{-3})
1.5, 100:0	33.7	1.43	3.59	1.61	2.42
1.5, 90:10	34.7	1.32	3.78	1.53	2.42
1.5, 80:20	34.1	2.57	4.01	1.51	2.54
1.5, 70:30	31.4	1.83	4.29	1.18	2.12
1.5, 60:40	31.6	1.62	4.63	1.40	2.72
1.5, 50:50	32.7	3.09	5.07	0.84	1.78
1.5, 40:60	34	0.4	5.67	1.08	2.56
1.5, 30:70	31	0.54	6.55	0.52	1.42
20, 80:20	31.8	0.05	1.10	0.60	0.28
40, 80:20	31.8	0.08	0.78	0.34	0.11
80, 80:20	31.8	147	0.55	3.51	0.81
120, 80:20	33	182	0.45	3.64	0.68
160, 80:20	31.5	0.75	0.39	13.3	2.15
20, 50:50	31.8	0.3	1.39	4.44	2.58
40, 50:50	31	0.23	0.98	2.08	0.86
80, 50:50	33.1	5240	0.69	3.52	1.02
120, 50:50	32.4	2460	0.57	3.64	0.86
160, 50:50	32.1	2310	0.49	5.29	1.09
20, 20:80					
40, 20:80	31.2	1.77	1.55	1.35	0.88
120, 20:80	30.6	134	0.90	3.66	1.37
160, 20:80	30.9	98	0.78	5.09	1.65

high and low curvature ethoxylates with mono and di-C_{12} quaternary ammonium bromides. Their study on $C_{12}E_2$ with single and dichain cationic showed that the solution microstructure was in the form of bilayers. They also found a solubility limit for $C_{12}E_2$ which is close to the region where phase separation is observed for DHDAB $C_{12}E_3$. Safinya and co-workers,[42] reported changes in bilayer rigidity with the addition of alkanol cosurfactants to the point where the bilayers become stabilized purely by undulation forces rather than by charge.[42,43] The variation in Caille parameter observed in the present work does not suggest that this limit is reached by the addition of $C_{12}E_3$, and the bilayers remain charge stabilized with relatively low Caille parameters up until the point where sufficient nonionic is added that phase separation occurs. Contrary to expectations the $C_{12}E_3$ has minimal effect on bilayer rigidity at low concentrations (~1 mM) and indeed stiffens the membranes at high solution concentration. At low concentration $C_{12}E_3$ prefers to form a separate aggregated phase in bulk solution when present at sufficiently high solution

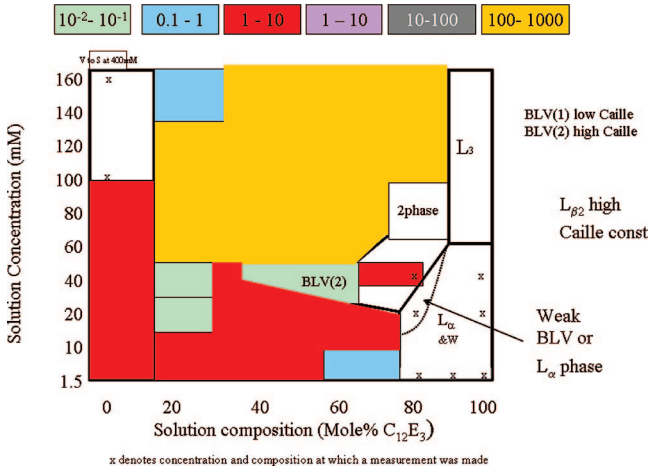

Figure 9. Phase diagram for DHDAB $C_{12}E_3$ based on the κB product derived from Nallet analysis. The color map represents the relative change in κB product, grouped by range. The data are the prefactors and should be multiplied by 10^{-9} ergs^2 cm^{-3}.

composition, suggesting an intrinsic incompatibility. Nieh et al. have studied the effect of adding charged lipids to phospholipid mixtures,[44] and have varied the solution conditions for these mixtures.[45] A range of solution microstructures are observed which are similar to those observed in the current system. However they did not observe a continuous lamellar phase at high solution concentration. The interlayer spacings derived from the Bragg scattering in that system are smaller than those observed in DHDAB $C_{12}E_3$, perhaps reflecting the particular properties of their chosen cosurfactant, and the fact that it has a larger spontaneous curvature.

5. Summary

The solution microstructure, at low concentrations and across the composition range 100:0 to 0:100 consists of three discrete regions; of bilamellar (100:0 to 80:20), multilamellar vesicles (80:20 to 30:70) and lamellar phase dispersion (30:70 to 0:100). The variations in the detail of the scattering and in optical texture with solution composition are relatively subtle. However, over a period of two years there is no evidence of macroscopic phase separation at any composition other than the 80:20 DHDAB $C_{12}E_3$ mixture. This suggests that if demixing into two coexisting lamellar phases is responsible for the observed bulk and surface phase behavior,[13,15] then the dynamics of demixing are infinitely slow. The fact that the 80 mM 80:20 sample phase separated only after storage for approximately 2 years implies that the bulk densities of the separate phases are sufficiently similar to each other that there is no overwhelming macroscopic manifestation of this effect. The variations in optical texture coincide with changes in the multilamellar vesicle structure and must therefore be due to changes in interaction forces between the particles and probably of electrostatic origin. The variations in membrane

(41) Blom, A; Warr, G. G. *Langmuir* **2006**, *22*, 6787.
(42) Safinya, C R; Sirota, E B; Roux, D; Smith, G S *Phys. Rev. Lett.* **1989**, *62*, 1134.
(43) Safinya, C R; Roux, D; Smith, G S; Sinha, S K; Dimon, P; Clark, N A; Bellocq, A M *Phys. Rev. Lett.* **1986**, *57*, 2718.
(44) Nieh, M-P.; Harroun, T. A.; Raghunathan, V. A.; Glinka, C. J.; Katsaras, J. *Biophys. J.* **2004**, *86*, 2615.
(45) Nieh, M-P.; Glinka, C. J.; Krueger, S.; Prosser, R. S.; Katsaras, J. *Biophys. J.* **2002**, *82*, 2487.

rigidity, derived from analysis of the scattering patterns are consistent with these different regions of the phase diagram, however the magnitude of the variations observed are not predicted using existing theoretical treatments.

Acknowledgment. We are grateful to the ISIS, ILL and NIST facilities for the provision of beam time, and to the instrument scientists for their support. There have been many significant discussions with Dr. E. J. Staples, formerly of Unilever Research, and they have contributed to some of the arguments presented here. Certain commercial equipment, instruments, or materials are identified in this paper; this does not imply recommendation or endorsement by the National Institute of Standards and Technology, nor does it imply that the materials or equipment identified are necessarily the best available for the purpose. This research has utilized facilities supported in part by the National Science Foundation under Agreement No. DMR-0454672.

Supporting Information Available: Details of the estimate of effective resolution on the two SANS instruments, the bulk aggregate compositions and evidence of phase separation in the 80 mM 80:20 DHDAB $C_{12}E_3$ mixture. This material is available free of charge via the Internet at http://pubs.acs.org.

LA8012359